Anal. Chem. **2010,** *82,* 3114–3117

Letters to *Analytical Chemistry*

Effects of Constant Voltage on Time Evolution of Propagating Concentration Polarization

Thomas A. Zangle, Ali Mani, and Juan G. Santiago*

Stanford University, Stanford, California 94305

We extend the analytical theory of propagating concentration polarization (CP) to describe and compare the effects of constant-voltage versus constant-current conditions on the transient development of CP enrichment and depletion zones. We support our analysis with computational and experimental results. We find that at constant voltage, enrichment and depletion regions spread as $t^{1/2}$ as opposed to the previously observed t^1 scaling for constant current conditions. At low, constant voltages, the growth and propagation of CP zones can easily be misinterpreted as nonpropagating behavior.

Recent work has shown that microfluidic−nanofluidic interfaces can be used to create preconcentration devices[1−4] or mixers[5] and that microfluidic−nanofluidic interfaces can have profound effects on sample transport throughout microchannel−nanochannel systems.[6−9] In particular, concentration polarization (CP) can create a redistribution of ionic strength which has a significant influence on analyte concentrations and electric fields in these devices.[10−13]

In a series of papers,[9,12,13] we showed that under certain conditions, CP enrichment and depletion regions can spread as shocks. For constant-current conditions this leads to linear (in time) growth of enrichment and depletion zones at a rate proportional to the applied current. Experimentally, we confirmed that CP propagation is driven by a long-range mechanism controlled by electromigration and not merely a diffusion phenomena. These studies and experiments were performed for constant-current conditions which more clearly and simply emphasize CP shock propagation physics.

The majority of experiments and computations have focused on constant-voltage conditions.[1,4−8,11,14] These have trends for growth of CP zones distinct from the constant current case, and several of these experimental studies have commented in detail on the transient and quasi-steady state behavior of CP at constant voltage.[6−8] In particular, at least some previous observations under constant voltage conditions[6,7] have concluded that CP ceased to propagate over time scales of 50−800 s. There is therefore a perceived discrepancy regarding the nature of constant current versus constant voltage cases. Analyses and experimental observations are needed to help reconcile these two different sets of observations.

In this letter, we consider the time evolution of CP in one-dimensional microchannel−nanochannel systems (as in Figure 1). We investigate this system under two applied power conditions: one case in which current is maintained constant and another (more common) case in which the voltage across the system is constant. We first present analysis based on the model of Mani et al.[12] and Zangle et al.[13] to gain intuition into the spread of CP enrichment and depletion zones at constant voltage. This analysis provides closed-form relations showing that, for large times, the enrichment and depletion regions in a constant-voltage experiment grow proportionally to the square root of time. We validate this prediction and compare it to the constant-current case using computational and experimental results. Finally, we use analysis and computations to show that at long times, the rate of thickening of the enrichment shock can match its propagation rate. This leads to growth which can be mistaken for simple diffusion or a nonpropagating form of CP but which is instead simply explained by an increasingly current-limited shock propagation phenomena.

ANALYTICAL MODEL

We present a simple one-dimensional analysis for the system shown in Figure 1. We draw on an existing model[12,13] but explore and expand on the special case of constant applied potential.

* To whom correspondence should be addressed. E-mail: juan.santiago@stanford.edu.

(1) Kim, S. M.; Burns, M. A.; Hasselbrink, E. F. *Anal. Chem.* **2006**, *78* (14), 4779–4785.
(2) Wang, Y.-C.; Stevens, A. L.; Han, J. *Anal. Chem.* **2005**, *77* (14), 4293–4299.
(3) Wang, Y.-C.; Han, J. *Lab Chip* **2008**, *8* (3), 392–394.
(4) Kim, P.; Kim, S. J.; Han, J.; Suh, K. Y. *Nano Lett.* **2009**, *10* (1), 16–23.
(5) Kim, D.; Raj, A.; Zhu, L.; Masel, R. I.; Shannon, M. A. *Lab Chip* **2008**, *8*, 625–628.
(6) Dhopeshwarkar, R.; Crooks, R. M.; Hlushkou, D.; Tallarek, U. *Anal. Chem.* **2008**, *80*, 1039–1048.
(7) Hlushkou, D.; Dhopeshwarkar, R.; Crooks, R. M.; Tallarek, U. *Lab Chip* **2008**, *8*, 1153–1162.
(8) Plecis, A.; Nanteuil, C.; Haghiri-Gosnet, A.-M.; Chen, Y. *Anal. Chem.* **2008**, *80*, 9542–9550.
(9) Zangle, T. A.; Mani, A.; Santiago, J. G. *Chem. Soc. Rev.* **2010**, *39*, 1014–1035.
(10) Pu, Q.; Yun, J.; Temkin, H.; Liu, S. *Nano Lett.* **2004**, *4* (6), 1099–1103.
(11) Kim, S. J.; Li, L. D.; Han, J. *Langmuir* **2009**, *25* (13), 7759–7765.
(12) Mani, A.; Zangle, T. A.; Santiago, J. G. *Langmuir* **2009**, *25* (6), 3898–3908.
(13) Zangle, T. A.; Mani, A.; Santiago, J. G. *Langmuir* **2009**, *25* (6), 3909–3916.
(14) Zhou, K.; Kovarik, M. L.; Jacobson, S. C. *J. Am. Chem. Soc.* **2008**, *130*, 8614–8616.

10.1021/ac100432q
Published on Web 03/29/2010

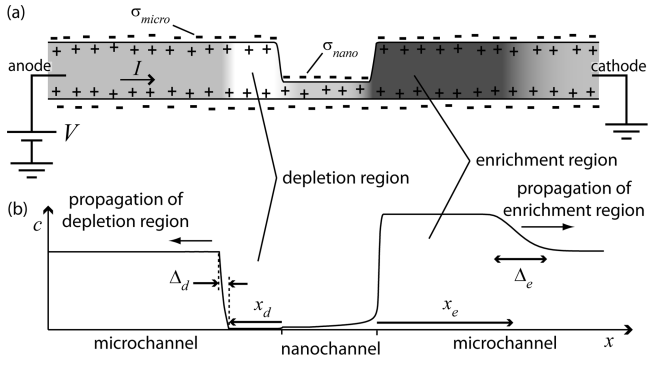

Figure 1. Schematic of the microchannel−nanochannel system: (a) system with an applied voltage, V, current of I, microchannel surface charge density of σ_{micro}, and nanochannel surface charge density of σ_{nano}. (b) Axial concentration distribution (matching the grayscale shading in part a), c, width of the enrichment and depletion regions, x_e and x_d, and enrichment and depletion shock thicknesses, Δ_e and Δ_d. c represents the concentration of the counterion to the wall charge outside of the electrical double layer (EDL) for nonoverlapped EDLs. For overlapped EDLs, c is the leading term of the Boltzmann distribution describing the concentration of ions through the EDL, c exp $(-z\zeta e/kT)$.

Previous work[12,13] showed that propagating CP enrichment and depletion fronts spread as shock waves with velocities linearly proportional to the current through the system. Furthermore, the shock thickness is inversely proportional to the difference of the characteristic ion transport velocities on either side of the shock and thus inversely proportional to the current:

$$\frac{\mathrm{d}}{\mathrm{d}t}x_\mathrm{d} \sim I \quad \text{and} \quad \Delta_\mathrm{d} \sim I^{-1} \tag{1}$$

where x_d and Δ_d represent the axial location and thickness of the depletion shock, respectively (see Figure 1). For constant current, this yields a constant-thickness shock advancing linearly in time as observed by Zangle et al.[13] In the constant-voltage case, however, the current through the system changes as CP dynamics modify the system resistance. As the depletion shock propagates, it trails a region of low conductivity which dominates overall impedance. The resistance of the system increases linearly with the axial length of this depleted region. Assuming the depletion shock interface is significantly smaller than the channel length

$$R_\mathrm{system}(t) \approx R_0 + Cx_\mathrm{d}(t) \tag{2}$$

where R_system represents the total electric resistance of the system, R_0 is the initial resistance, and C represents the resistance per unit length of the growing depletion region. In eq 2, we neglect the decrease of resistance due to growth of the enrichment region relative to the effect of the depletion growth. This is because typically the increase in concentration inside the enrichment region is of order unity, whereas the concentration in the depletion region is orders of magnitude lower than the initial concentration.[12,13] Using eq 2 to express the resistance of the system, we can rewrite eq 1 as

$$\frac{\mathrm{d}}{\mathrm{d}t}x_\mathrm{d} \sim \frac{V}{R_\mathrm{system}} \tag{3}$$

where V is the applied voltage. Substituting eq 2 into eq 3 yields the following differential equation for x_d:

$$\frac{\mathrm{d}}{\mathrm{d}t}\left(R_0x_\mathrm{d} + \frac{1}{2}C{x_\mathrm{d}}^2\right) \approx V \tag{4}$$

Over sufficiently long times (when $Cx_\mathrm{d} \gg R_0$), the second term on the left-hand side of eq 4 dominates the first term and this leads to the following scaling for shock location:

$$\frac{\mathrm{d}}{\mathrm{d}t}x_\mathrm{d} \sim t^{1/2} \tag{5}$$

Therefore, at long times the resistance of the depletion region dominates and I scales as V/x_d. From eq 1 this leads to the following scaling for the shock thickness:

$$\Delta_\mathrm{d} \sim t^{1/2} \tag{6}$$

Note that here we implicitly assumed that the shock structure has a fast response to instantaneous changes in current. A similar analysis (again assuming that the depletion shock dominates the total resistance) for the enrichment shock location and thickness yields

$$\frac{\mathrm{d}}{\mathrm{d}t}x_\mathrm{e} \sim t^{1/2}, \quad \Delta_\mathrm{e} \sim t^{1/2} \tag{7}$$

From eqs 5−7, we see that shock advancement and thickening are both proportional to $t^{1/2}$. Under certain conditions (i.e., low enough Peclet number, $Pe_L = U_\mathrm{b}L/D$, where L is the characteristic axial channel length, U_b is the bulk velocity, and D is ion diffusivity), the theoretical rate of shock thickening can be on the order of the propagation rate. In this case, a moving "shock" structure (i.e., a sharp interface propagating away from the microchannel−nanochannel interface) is not clearly observed. Instead, the system's response is that of a gradually slowing and thickening enrichment interface. Over a sufficiently long time ($t \sim (L/D)^{0.5}$), the growth of enrichment and depletion zones will be arrested by diffusive interaction with the end-channel reservoirs.

For higher Pe_L, this scaling predicts growth of the depletion region as $t^{1/2}$, where shock widths are much smaller than the axial width of enrichment/depletion zones. In this case, the shock scale can be distinguished from the propagation scale, although both grow as $t^{1/2}$. Below, we verify the simple asymptotic behaviors predicted here using experiments and computations.

COMPUTATIONAL MODEL

Figure 2 presents computational results for both constant-current and constant-voltage cases from the code and numerical scheme described in Zangle et al.[13] Figure 2a shows a 1 mM initial concentration, and Figure 2b shows a 250 μM initial concentration. In constant voltage simulations, we rescale the input current at each time step to maintain a specified voltage between the ends of the channel system. This rescaling is justified as the relation between the current and voltage is linear (see Mani et al.,[12] eq 22).

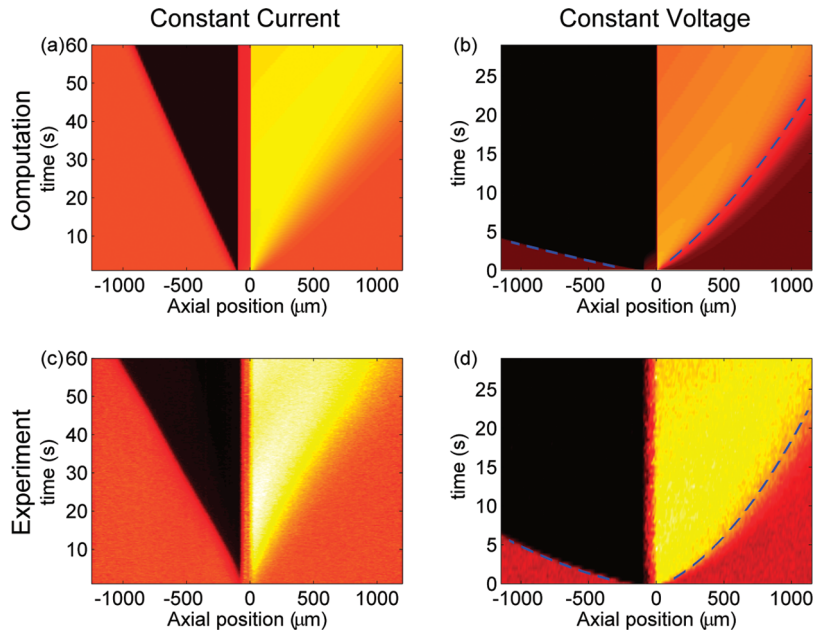

Figure 2. Computational and experimental results showing spatiotemporal plots for constant current and constant applied voltage. Computations are shown in the top row, experiments in the bottom row. The first column shows computational and experimental results for constant-current (800 pA) conditions. The second column shows constant-voltage (100 V) results. In these spatiotemporal plots, the distance is plotted on the *x*-axis, time on the *y*-axis, and the color map corresponds to concentration (yellow/white is high, black is low). The 100 μm long nanochannel starts at $x = 0$. Constant-current conditions (a, c) show a roughly linear spread of enrichment and depletion shocks with time while constant voltage conditions (b, d) show a parabolic spread of enrichment and depletion shocks, as predicted by theory. Parabolic least-squares best fit lines ($t = Ax^2 + Bx + C$) to contours of $c = 0.6c_{max}$ and $c = 0.05c_{max}$ are shown as dashed, blue lines in parts b and d.

As in Zangle et al.,[13] we used wall surface charge density inside the nanochannel, σ_{nano}, as the only fitting parameter between theory and experiments. The wall charge inside the microchannel, σ_{micro}, was set equal to the value determined by independent ζ-potential measurements. In Figure 2a, $\sigma_{nano} = 0.25\sigma_{micro}$, and in Figure 2b, $\sigma_{nano} = \sigma_{micro}$. All other parameters (including channel height, initial concentration, ion mobilities, and diffusivities) were set equal to experimental values based on independent measurements reported previously.[13]

The constant current results in Figure 2a show linear growth of enrichment and depletion regions with time (shock fronts are linear on the spatiotemporal plot). In contrast, the constant voltage results in Figure 2b show curved, parabolic spreading of enrichment and depletion regions with time. We show parabolic fits to contours of $c = 0.6c_{max}$ and $c = 0.05c_{max}$ (dashed blue curve), which have R^2 values of 0.9996 and 0.994, respectively, indicating the scaling of the dynamics is well predicted by eqs 5 and 7.

Figure 3 shows computational results at applied voltages of 10, 100, and 1000 V, for the same conditions as those of Figure 2b. For all of these cases, the analytical theory of Mani et al.[12] predicts propagating CP. At high voltages (1000 V in this case), the enrichment shock thickness, Δ_e, remains small relative to the enrichment region width, x_e, and this shock clearly propagates over long times. At lower voltages (10 V in this case), the growth of the CP enrichment region is slow relative to thickening of the enrichment shock. In this case, the enrichment region shock velocity slows down considerably, resulting in a long time condition where $t^{1/2}$-type growth of the interface width dominates. These results suggest that prior observations of CP at constant voltage in which the enrichment front appeared to gradually slow or stop[6,7] are

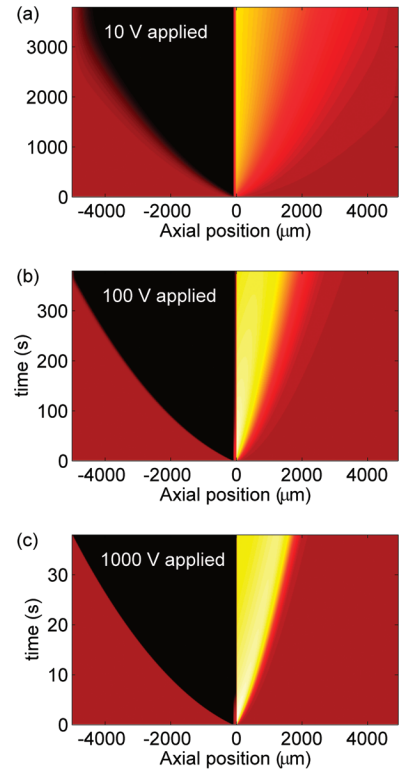

Figure 3. Computational results for applied potentials of (a) 10, (b) 100, and (c) 1000 V, at otherwise the same conditions as in parts c and d of Figure 2. At low voltage, the results show that (a) thickening of the enrichment shock dominates the spread of the enrichment region and the shock slows drastically and may be mistakenly reported to stop moving. At high voltage, (c) the shock thickness is small relative to the size of the growing enrichment region and the shock clearly propagates to the cathode side reservoir.

consistent with the model of Mani et al.[12] and Zangle et al.[13] and can be explained by strong initial propagation followed by $t^{1/2}$-type decay of propagation velocity and $t^{1/2}$ growth of interface width. Note that diffusion plays an important role, but this process is primarily due to the coupling of shock dynamics and the decreasing current associated with constant voltage.

EXPERIMENTAL MEASUREMENTS

We also performed a series of new experiments at constant applied voltage to test the predictions of eqs 5 and 7. Details of the channel design and fabrication are described in Zangle et al.[13] We filled a series of microchannel−nanochannel−microchannel devices with either 1 mM (Figure 2c) or 250 μM (Figure 2d) Alexa Fluor 488 dye in deionized water. With this system, we can directly observe the behavior of the background electrolyte (the fluorescent Alexa Fluor species and its lithium counterion) using epifluorescent microscopy.[13]

Figure 2c shows experimental results for a constant 800 pA current in a system with an initial concentration of 1 mM Alexa Fluor 488. At this condition, the enrichment and depletion shocks move at nearly constant velocity as predicted by theory and in agreement with the computations presented in Figure 2a.

Figure 2d shows experimental results for a channel initially filled with 250 μM Alexa Fluor 488 at a constant voltage of 100 V. This result shows an enrichment front migrating as $t^{1/2}$ as predicted by eq 5 and consistent with the computational results in Figure 2b. The R^2 values for the parabolic best fit line to $c = 0.6c_{max}$ (210 points) and the $c = 0.05c_{max}$ (45 points) contours were, respectively, 0.999 and 0.991. These fits are plotted in Figure 2d as dashed lines. The goodness-of-fit of these parabolas confirm the prediction of eq 7 that in a constant-voltage experiment, CP enrichment shocks spread as $t^{1/2}$.

SUMMARY

We presented a brief, analytical derivation which draws on the model of Mani et al.[12] showing that under constant-voltage conditions, CP enrichment and depletion regions have propagation velocities which scale as $t^{1/2}$ while the enrichment and depletion shock thicknesses grow as $t^{1/2}$. This transient behavior is, of course, limited to the time until these moving boundaries start interacting with the reservoirs and/or electrodes at the boundaries. As such, the duration of these events is a function of channel lengths and applied current densities. Using new computations and experiments, we confirmed this scaling derivation and the parabolic spatiotemporal growth of the width of CP enrichment and depletion regions for constant-voltage conditions. Computations for low applied voltage show that at long times and low Peclet numbers, the growth of CP enrichment and depletion regions is slow relative to shock thickening. This $t^{1/2}$ shock thickening can be mistaken for an arrested (stopped) propagation of CP enrichment and depletion regions or for a simple one-dimensional diffusion-dominated process. Instead, this $t^{1/2}$ growth of the shock interface width is due to a coupling of the shock propagation dynamics (in which diffusion plays a key role) and the gradual decrease in current due to constant applied voltage and the growing depletion region. Together, these results help explain the distinctly different observations of CP at constant voltage versus constant current conditions.

Received for review February 16, 2010. Accepted March 24, 2010.

AC100432Q